

Electromagnetic excitation of ultrasound in a dysprosium single crystal

A. V. Andrianov, V. D. Buchel'nikov, A. N. Vasil'ev, Yu. P. Gaïdukov, and V. G. Shavrov

Moscow State University

(Submitted 29 December 1989; resubmitted 23 January 1990)

Zh. Eksp. Teor. Fiz. **97**, 1674–1687 (May 1990)

The magnetic-field dependence of the efficiency of electromagnetic excitation of longitudinal ultrasound in a dysprosium single crystal was investigated in a temperature range including the regions where the ferromagnetic ($T > T_1$), antiferromagnetic ($T_1 < T < T_2$), and paramagnetic ($T > T_2$) states exist. It is observed that for $T < T_2$ the domain-wall displacements as well as the rotation of the magnetization vector in the domains are accompanied by intense generation of ultrasound. Intense sound generation is observed in the interval $T_1 < T < T_2$ in transitions from the antiferromagnetic to the ferromagnetic phase, as well as in the entire region where the intermediate ferromagnetic phase exists. The magnetic phase diagrams of Dy are plotted for a magnetic field oriented in the basal plane along the directions of the easy and hard magnetization.

1. INTRODUCTION

The changes produced in the spin subsystem of a magnet by an external magnetic field or by temperature are manifested in many interactions, particularly magnetoelastic ones. To study these interactions one can use the phenomenon of electromagnetoacoustic transformation (EMAT) on the magnet boundary.¹ A distinctive feature of this phenomenon, compared for example with the conventional methods of investigating magnetostriction, is that the amplitude of the sound excited by the electromagnetic wave in the skin layer of the metal is determined not only by the values of the magnetoelastic coefficients, but also by the elastic, magnetic, and electric properties of the substance. Thus, intense generation of elastic waves is possible only when the wavelength of the excited ultrasound exceeds substantially the depth of penetration of the electromagnetic waves in the metal. The EMAT is determined in a wide range of frequencies, magnetic fields, and temperatures by various interactions. In magnetically ordered media, however, the principal role is assumed by the interaction between the magnetic and elastic subsystems.

A theoretical description of EMAT in Dy presupposes an analysis, first, of the rotation of the magnetization vectors in the domains, and second, of the transitions between various magnetic states, including transitions from the helicoidal antiferromagnetic phase into various ferromagnetic phases. EMAT efficiency peaks in transitions from the antiferromagnetic to the paramagnetic or ferromagnetic phase were observed earlier in polycrystalline Dy samples.² They are qualitatively attributed to an increase of the magnetic susceptibility of the metal, whereas the parameters of the magnetically ordered coupling remain practically unchanged.

We report here an experimental investigation of EMAT of single-crystal Dy having a hexagonal crystal structure. The single-axis magnetic anisotropy of Dy is so strong that when it is magnetically ordered the moments are always oriented in the basal plane. In the absence of a magnetic field, as temperature increases dysprosium goes over from a ferromagnetic phase of the "easy plane" type at $T_1 = 85$ K into a helicoidal antiferromagnetic phase of the "simple spiral" type, and then at $T_2 = 180$ K into the paramagnetic phase.³ For $T < T_1$, application of a magnetic field in the basal plane ab produces the usual ferromagnet magnetization produced

by displacement of the domain walls and rotation of the magnetization vectors in the domains. In the interval $T_1 < T < T_2$ application of a magnetic field destroys the antiferromagnetic spiral. Investigations of the influence of a magnetic field oriented along the a axis on the magnetization,⁴ conductivity,⁵ and the speed of sound⁶ in Dy have shown that destruction of the antiferromagnetic spiral is accompanied by formation of an intermediate "fan" ferromagnetic phase.

The field dependence of the EMAT efficiency was used in the present study to determine the limits of existence of various magnetic phases in Dy. The H - T diagram obtained for $\mathbf{H} \parallel \mathbf{a}$ practically coincides with the data of Refs. 4–6; the measurements for $\mathbf{H} \parallel \mathbf{b}$ were made here for the first time (\mathbf{a} and \mathbf{b} are, respectively, the easy- and difficult-magnetization axes in the basal plane). A brief report of the experimental results of this study is contained in Ref. 7.

2. MEASUREMENT METHOD

The Dy single crystal investigated in the present study was a parallelepiped measuring 0.435, 0.58, and 0.33 cm along the c , b , and a axes, respectively. The sample purity was characterized by the resistance ratio $R(293)/R(4.2) = 88$. The sample was placed in a rectangular inductance coil to which were applied rf pulses of amplitude ≈ 2 keV, duration $\approx 1 \mu\text{sec}$, and carrier frequency 10 MHz. An external magnetic field \mathbf{H} of intensity up to 70 kOe was applied to the basal plane (along either the \mathbf{a} or \mathbf{b} axis) parallel to the oscillatory magnetic field \mathbf{h} produced by the coil ($h \sim 10^2$ Oe). At 10 MHz the wavelength of the excited sound is ten times smaller than the geometric dimensions of the samples, so that the elastic waves propagating in the crystal can be regarded as practically plane.

The oscillations excited in the sample were recorded with the same coil by using the inverse EMAT effect on the metal boundary. The measurements were made by an echo method, with the signal from the third or fourth reflected ultrasound pulse recorded. In this experimental setup the signal is proportional to the square of the amplitude of the excited sound or, equivalently, to the conversion efficiency K (Ref. 8). In most cases the $K(H)$ dependences were plotted at constant temperature. To determine the limits of existence of various magnetic states in Dy, we measured in some cases combined temperature-field dependences: the mag-

netic field was varied with temperature in accordance with a prescribed program, so that the EMAT efficiency could be plotted for motion in the H - T plane along a chosen path.

The inductance coil surrounding the sample was used also to plot the field dependence of the sample magnetization by the fluxmeter method. The sample and the coil that encloses it were placed in a helium cryostat in the "warm field" channel of the superconducting solenoid. The temperature was monitored to within 1 K with a Cu-CuFe thermocouple.

3. EXPERIMENT

3.1. Ferromagnetic region $T > T_1$

Families of characteristic field dependences of the EMAT efficiency K , obtained for two orientations of the constant magnetic field ($\mathbf{H} \parallel \mathbf{a}$ and $\mathbf{H} \parallel \mathbf{b}$) are shown for a number of temperatures in Figs. 1 and 2, respectively. Figure 2 shows also the typical field dependence $M(H)$ of the magnetization [the $K(H)$ curves are drawn to various scales, and the attenuation coefficients in dB are indicated in the figure captions for each curve].

We consider first the $K(H)$ dependence obtained in the ferromagnetic phase of dysprosium for $T < T_1$ (curve 1 in Fig. 1 and curves 1 and 2 in Fig. 2). For $\mathbf{H} \parallel \mathbf{a}$ only one generation peak is observed in the region of relatively weak magnetic fields: the EMAT signal appears in the field H_1 practically simultaneously with the start of application of the magnetic field ($H_1 \approx 0$), reaches a maximum at $H \approx 10$ kOe, and then decreases rapidly. The character of these curves remains practically unchanged with change of temperature.

In a magnetic field oriented along the difficult magnetization axis ($\mathbf{H} \parallel \mathbf{b}$), the field dependence of the EMAT

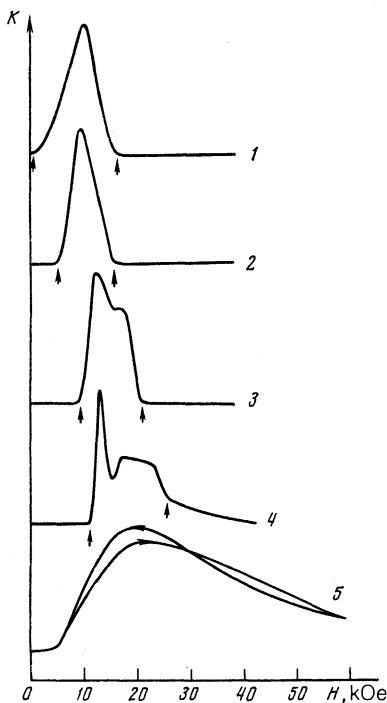


FIG. 1. Plots of EMAT efficiency $K(H)$ vs the external magnetic field at $\mathbf{H} \parallel \mathbf{a}$: 1— $T = 82$ K, attenuation 0 dB; 2—119 K, 5 dB; 3—141 K, 15 dB; 4—172 K, 21 dB; 5—181 K, 12 dB. The arrows show the fields of the start and end, designated in the text by H_1 and H_2 , respectively, of the effective ultrasound excitation.

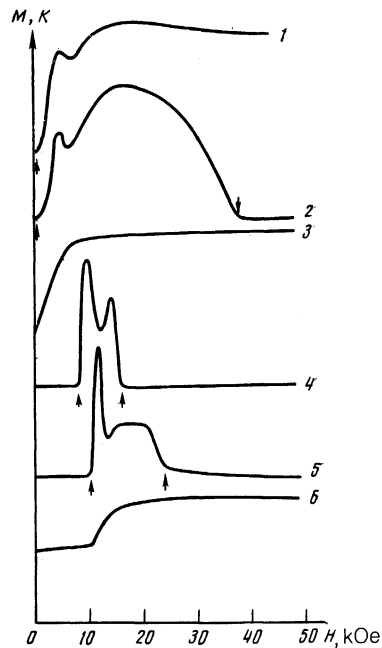


FIG. 2. Plots of $K(H)$ and $M(H)$ at $\mathbf{H} \parallel \mathbf{b}$. $K(H)$: 1— $T = 50$ K, attenuation 0 dB; 2—70 K, 11 dB; 4—136 K, 24 dB; 5—173 K, 37 dB, $M(H)$: 3— $T = 70$ K; 6—173 K. The arrows mark the fields H_2 and H_1 .

shows, following the generation peak in weak fields ($H \approx 10$ kOe), intense generation in a wide range of magnetic fields, which terminates with the field H_1 . The field H_2 increases rapidly when the temperature is lowered. As for the field dependence of the magnetization for $T < T_1$, it is practically the same for both \mathbf{H} orientations: in weak field the magnetization undergoes a rapid growth that ends in a field approximately corresponding to the EMAT maximum in weak fields, after which the $M(H)$ curve reaches saturation (curve 3 of Fig. 2).

The interpretation of the EMAT field dependence for $T < T_1$ is given in Sec. 4.2. It reduces qualitatively to the following. In the customarily assumed weak field the sample contains six types of domain, and the internal field in the magnet is weak. Generation of longitudinal sound for $\mathbf{H} \parallel \mathbf{a}$ is due only to domain-wall displacements: when the magnetic field is increased, the volume of the domains in which $\mathbf{M} \parallel \mathbf{H}$ increases and the volume of the domains in which the vector \mathbf{M} is either antiparallel to \mathbf{H} or makes an angle with it decreases. Modulation of the constant magnetic field by an rf field in the sample skin layer leads, on account of the magnetoelastic coupling, to excitation of ultrasound. After the sample goes over into the collinear single-domain phase, the sample is magnetized to saturation and the EMAT efficiency decreases steeply.

In the $\mathbf{H} \parallel \mathbf{b}$ orientation the sample magnetization should be completed by aligning the magnetization vector in the domain with the direction of the difficult axis \mathbf{b} . The sequence of the ensuing changes of the dysprosium magnetic state is the following. The displacement processes, as in the preceding case, lead to excitation of ultrasound and to appearance of a peak on the $K(H)$ plot in the region of weak magnetic fields. After the displacement processes terminate, there remain in the sample two types of domain, in which the vector \mathbf{M} makes an angle 30° with the magnetic field. Addi-

tional magnetization of the crystal, up to the field H_2 , is due to rotation of the vectors \mathbf{M} in these domains. This magnetic state will hereafter be called the oblique phase. Effective EMAT takes place also in the angle phase. The magnetic-field interval in which sound generation is observed is determined by the constant $K_0(T)$ of the easy-axis anisotropy.

3.2. Antiferromagnetic region $T_1 < T < T_2$

In the temperature interval $T_1 < T < T_2$ the general character of the $K(H)$ dependences (curves 2–4 in Fig. 1 and curves 4, 5 in Fig. 2) is the following: in weak fields, up to a certain value that depends on the temperature-dependent field H_1 , the magnetization changes little, and no excitation of ultrasound is registered. When the field H_1 is reached, the slope of the $M(H)$ curve increases abruptly and an EMAT signal appears discontinuously. After the $K(H)$ peak, there can be produced near H_1 an entire region of intense excitation of ultrasound, extending all the way to the field H_2 , which is also temperature-dependent. No EMAT is registered in fields stronger than H_2 , and the magnetization saturates. The field dependences of the EMAT of this type are typical of both investigated orientations of the external magnetic field.

The $K(H)$ and $M(H)$ dependences obtained at $T_1 < T < T_2$ offer evidence that the destruction of the antiferromagnetic helicoid goes through two stages. The sequence of the magnetic states is then the following: for $H < H_1(T)$ the antiferromagnetic helix is preserved, while in fields $H \gtrsim H_1(T)$ it is destroyed and an intermediate ferromagnetic phase is formed and preserved up to the field $H_2(T)$. In fields $H > H_2(T)$ all the magnetic moments take the direction of the magnetic field and the sample is magnetized to saturation. One should accordingly observe on the field dependence of the magnetization weakly pronounced slope changes, while the $K(H)$ curves should show peaks of ultrasound generation when the antiferromagnetic spiral and the regions of intense sound generation are destroyed by spin reorientation in the intermediate ferromagnetic phase.

3.3. Intermediate-phase region

A natural question concerns the character of the intermediate ferromagnetic phase. In a field $\mathbf{H} \parallel \mathbf{b}$ for $T < T_1$, an oblique phase is certainly produced after the completion of the displacement, and a fan phase is apparently realized at $T \lesssim T_2$ —after the destruction of the antiferromagnetic helicoid (see Sec. 5). There should exist therefore between these two phases a separation region (or boundary). To find the suggested boundary, detailed measurements of the EMAT were undertaken at $T \gtrsim T_1$. These measurements were made both by drawing combined plots against the temperature and field, and by plotting field dependences at a fixed temperature. Their distinctive feature, as shown in Fig. 3, is the appreciable hysteresis which is absent at low temperatures. It can be assumed that the line on the H - T diagram that demarcates the regions with and without hysteresis on the $K(H)$ plot is the boundary of the oblique phase. An analysis of the intermediate state is given in Sec. 5 below.

3.4. Paramagnetic region $T > T_2$

Finally, for $T > T_2$, the EMAT plots show one broad generation maximum whose value decreases with increasing distance from the T_2 (curve 5 of Fig. 1). This behavior is

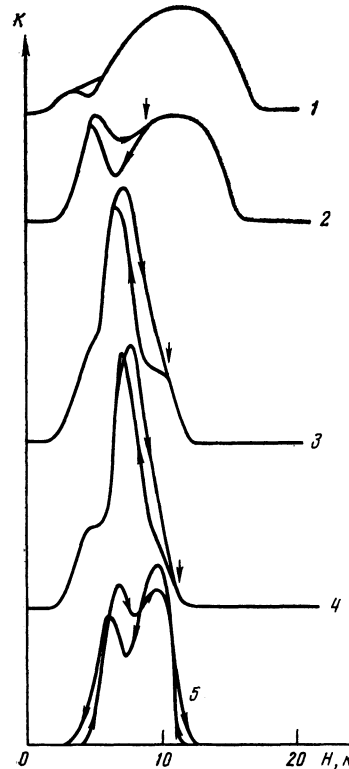


FIG. 3. Plots of $K(H)$ at $\mathbf{H} \parallel \mathbf{b}$: 1— $T = 91$ K; 2— 92 K; 3— 98.5 K; 4— 101 K; 5— 119 K the arrows mark the fields at which the hysteresis processes terminate.

typical of the paramagnetic phase of any magnet, and an interpretation for it is given, e.g., in Ref. 9. Note that near T_2 the paramagnetic phase of Dy also has hysteresis on the EMAT field dependences.

4. THEORY

Generation of longitudinal sound by spin reorientation in a single-domain magnet was investigated theoretically and experimentally in Gd single crystals.⁹ The equations obtained in Ref. 9 can be used, but only to describe the rotation of the magnetization vectors in single-domain samples. We consider below the peculiarities of sound generation following restructuring of the domain in dysprosium.

4.1. Sound generation following spin reorientation in a polydomain magnet

Assume that the metal contains two types of domain of equal size and with magnetizations symmetrically directed relative to the external field \mathbf{H} . The sample magnetization is effected here only by rotation of the magnetization vectors in the domains in the \mathbf{H} direction. The free energy density F of the magnet can be expressed in this case in the form

$$F = \sum_{\alpha=1}^2 \left[-\frac{1}{4} K_1 \cos^2 \theta_\alpha - \frac{1}{8} K_2 \cos^4 \theta_\alpha - \frac{1}{2} K_3 \sin^6 \theta_\alpha \cos 6\varphi_\alpha - \frac{1}{2} M_s H \sin \theta_\alpha \sin \varphi_\alpha - \frac{1}{2} \mathbf{h} \mathbf{M}^\alpha + \frac{1}{2} \gamma_{ijk} M_i^\alpha M_j^\alpha U_{kl} \right] + c_{ijk} U_{ij} U_{kl} + \frac{1}{8} M_s^2 [N_1 (\sin \theta_1 \cos \varphi_1 + \sin \theta_2 \cos \varphi_2)^2 + N_2 (\sin \theta_1 \sin \varphi_1 + \sin \theta_2 \sin \varphi_2) + N_3 (\cos \theta_1 + \cos \theta_2)^2] + \frac{1}{2} \pi M_s^2 (\sin \theta_1 \sin \varphi_1 - \sin \theta_2 \sin \varphi_2)^2. \quad (1)$$

Here θ_2 and φ_3 are the polar and azimuthal angles of the magnetization in the domains, K_i , γ_{ijkl} , c_{ijkl} are respectively, the constants of the anisotropy, the anisotropic relativistic magnetostriction, and the elasticity, \mathbf{M}^a is the magnetization in the domains, M_i^a are its components, M_s is the saturation magnetization, \mathbf{h} is the oscillating magnetic field, U is the strain tensor, and N_i are the sample demagnetizing factors. The next-to-last term in (1) is the demagnetization energy, and the last is the energy connected with the onset of magnetic charges on the domain walls.¹⁰ We have neglected in (1) the inhomogeneous exchange energy.

We consider the following relative orientation of the magnetic fields \mathbf{H} and \mathbf{h} and of the wave vector $\mathbf{k}:\mathbf{H}\parallel\mathbf{h}\parallel\mathbf{y}$, $\mathbf{k}\parallel\mathbf{n}\parallel\mathbf{x}$, where \mathbf{n} is the vector normal to the sample surface ($\mathbf{y}\parallel\mathbf{b}$, $\mathbf{x}\parallel\mathbf{a}$).

In investigations of ultrasound generation in magnets with domain structure (i.e., with inhomogeneous magnetization in the ground state) the equations of Landau and Lifshitz, of Maxwell, and of elasticity theory must be supplemented by the Saint Venant strain compatibility condition principle,¹⁰ which lead also to inhomogeneous strains in the ground state. However, if the domain-wall width is small compared with the period of the domain structure, the magnetization and strains inside the domains can be regarded as homogeneous. In this case the Landau-Lifshitz and elasticity equations lead, for a magnet in the ground state, to $\theta_1 = \theta_2 = \Theta = \pi/2$, $\varphi_1 = \Phi$, $\varphi_2 = \pi - \Phi$,

$$\begin{aligned} U_{xx,yy} &= -\frac{(G_{11}-G_{12})c_{33}}{2\Delta} \mp \frac{G_{11}-G_{12}}{2(c_{11}-c_{12})} \cos 2\Phi, \\ U_{zz} &= -c_{13}(U_{xx}+U_{yy})/c_{33}, \\ U_{xy} &= -\frac{G_{11}-G_{12}}{2(c_{11}-c_{12})} \sin 2\Phi, \quad U_{xz}=U_{yz}=0, \end{aligned} \quad (2)$$

where

$$\Delta = c_{33}(c_{11}+c_{12}) - 2c_{13}^2, \quad G_{ijkl} = \gamma_{ijn} M_s^2.$$

The azimuthal angle Φ is determined from the equation

$$6K_6 \sin 6\Phi - M_s H \cos \Phi + \frac{1}{2} M_s^2 N_2 \sin 2\Phi = 0. \quad (3)$$

The state with the domain structure (2) is stable at $H < H_{th}$, where the threshold field is

$$H_{th} = 36K_6/M_s + N_2 M_s. \quad (4)$$

At $H = H_{th}$ an orientational second-order transition takes place from a noncollinear state with a domain structure (2) into a collinear single-domain state with $\varphi_1 = \varphi_2 = \pi/2$.

For the propagation of an electromagnetic wave along the x axis, a system of equations linearized in the standard manner about the equilibrium position (2), (3) can be written as:

$$\begin{aligned} (1 - \frac{1}{2} i \delta^2 D^2) h_z - 4\pi M_s \theta_+ &= 0, \\ (1 - \frac{1}{2} i \delta^2 D^2) h_y + 4\pi M_s \varphi_- \cos \Phi &= 0, \\ \dot{\varphi}_+ &= \omega_1 \theta_+ + g h_z, \\ \dot{\theta}_+ &= -\omega_3 \varphi_+ - g(G_{11} - G_{12}) D u_y M_s^{-1} \cos 2\Phi, \\ \dot{\varphi}_- &= \omega_4 \theta_- - g G_{11} D u_z M_s^{-1} \cos \Phi, \\ \dot{\theta}_- &= -\omega_2 \varphi_- + g h_y \cos \Phi + g(G_{11} - G_{12}) D u_x M_s^{-1} \sin 2\Phi, \\ \rho \ddot{u}_x &= -(G_{11} - G_{12}) D \varphi_- \sin 2\Phi + c_{11} D^2 u_x, \\ \theta_{\pm} &= (\theta_1 \pm \theta_2)/2, \quad \varphi_{\pm} = (\varphi_1 \pm \varphi_2)/2, \quad D = \partial/\partial x, \quad \dot{\varphi} = \partial\varphi/\partial t, \end{aligned} \quad (5)$$

where

$$\begin{aligned} \theta_{\pm} &= (\theta_1 \pm \theta_2)/2, \quad \varphi_{\pm} = (\varphi_1 \pm \varphi_2)/2, \\ D &= \partial/\partial x, \quad \dot{\varphi} = \partial\varphi/\partial t, \end{aligned}$$

ρ is the density of the metal, g is the gyromagnetic ratio, and δ is the skin-layer thickness in nonmagnetic metal. The frequencies ω_i are given by the equations

$$\begin{aligned} \omega_1 &= \frac{g}{M_s} (-\tilde{K}_1 + 6K_6 \cos 6\Phi + M_s H \sin \Phi - M_s^2 N_2 \sin^2 \Phi + M_s^2 N_3), \\ \omega_2 &= \frac{g}{M_s} [36K_6 \cos 6\Phi + M_s H \sin \Phi + M_s^2 N_2 \cos 2\Phi + 2(G_{11} - G_{12})^2 / (c_{11} - c_{12})], \\ \omega_3 &= \omega_2 + 4\pi g M_s + g M_s (N_1 \sin^2 \Phi - N_2 \cos^2 \Phi), \\ \omega_4 &= \omega_1 - g M_s N_3, \end{aligned} \quad (6)$$

where \tilde{K}_1 is the renormalized first anisotropy constant.

The system (5) becomes much simpler if we set $\dot{\theta} = \dot{\varphi} = 0$. This condition is well satisfied when the frequency of the excited oscillations satisfies the inequality $\omega \ll \omega_i$. It is valid also at the transition point (4) where the frequency ω_2 is a minimum and equal to the magnetoelastic gap¹¹

$$\omega_{me} = 2g(G_{11} - G_{12})^2 / M_s (c_{11} - c_{12}).$$

In this approximation the variable magnetic field h_y excites only oscillations of spin waves φ_- and the longitudinal ultrasound u_x :

$$\begin{aligned} (1 - \frac{1}{2} i \delta^2 D^2) h_y + 4\pi M_s \varphi_- \cos \Phi &= 0, \\ \varphi_- &= \frac{g \cos \Phi}{\omega_2} h_y + \frac{g(G_{11} - G_{12})}{M_s \omega_2} D u_x \sin 2\Phi, \\ (\omega^2 + S_l^2 D^2) u_x &= \frac{1}{\rho} (G_{11} - G_{12}) D \varphi_- \sin 2\Phi, \end{aligned} \quad (7)$$

where $S_l^2 = c_{11}/\rho$.

The system (7) leads to a dispersion equation, similar to that found in Ref. 9, for coupled, spin, and elastic waves. In the case of a skin layer that is thin compared with the length of the elastic wave its solutions are two values of the wave number:

$$k_1 = \frac{1-i}{\delta} \left(\frac{\mu - \xi}{1 - \xi} \right)^{1/2}, \quad (8)$$

$$k_2 = k_2' - i\Gamma, \quad (9)$$

where

$$\begin{aligned} \mu &= 1 + 4\pi\chi = 1 + \frac{4\pi g M_s}{\omega_2} \cos^2 \Phi, \\ \xi &= \frac{g(G_{11} - G_{12})^2}{M_s c_{11} \omega_2} \sin^2 2\Phi = \frac{4(G_{11} - G_{12})^2}{M_s^2 c_{11}} \chi \sin^2 \Phi, \\ k_2' &= \frac{\omega}{S_l} \left(\frac{\mu}{\mu - \xi} \right)^{1/2} = \frac{\omega}{S_l}, \\ \Gamma &= \frac{\delta^2 \omega^2 k_2' (\mu - 1) \xi}{4S_l^2 (\mu - \xi)^2}. \end{aligned} \quad (10)$$

Equations (7) with boundary conditions for the stress tensor and for the vectors \mathbf{E} and \mathbf{H} on the free surface of the metal ($x = 0$) allow us to express the amplitude of the excited longitudinal sound u_{x2} in terms of the amplitude h_{oy} of the electromagnetic wave incident on the metal surface:

$$u_{0x} = \frac{\delta^2 \omega h_{0y}}{2S_l} \left[\frac{\mu(\mu-1)\zeta}{\pi(\mu-\zeta)^3 c_{11}} \right]^{1/2}. \quad (11)$$

Using this relation, we can find the rate of transformation of electromagnetic waves into elastic ones. The EMAT efficiency K is defined as the ratio of the fluxes of the acoustic

$$W_{ac} = \rho u_{0x}^2 \omega^2 S_l / 2$$

and electromagnetic

$$W_{em} = c h_{0y}^2 / 8\pi$$

energies on the metal boundary $x = 0$:

$$K = \frac{W_{ac}}{W_{em}} = \frac{S_l}{c} \left(\frac{\delta \omega}{S_l} \right)^4 \frac{\zeta(\mu-1)\mu^{1/2}}{(\mu-\zeta)^{5/2}}. \quad (12)$$

The EMAT efficiency is thus expressed in terms of the magnetoelastic-interaction parameter ζ and the dynamic magnetic permeability μ . According to (10), ζ and μ depend on the value of H , since this field governs the frequency ω_2 and the angle Φ in (10) [see Eqs. (3) and (6)]. Assuming the parameter ζ to be small compared with μ in the entire investigated interval of temperatures and magnetic fields, we get

$$K = \text{const} \frac{\chi_0^2 \sin^2 \Phi \cos^4 \Phi}{(1 + 4\pi\chi_0 \cos^2 \Phi)^2}, \quad (13)$$

where $\chi_0 = gM_s / \omega_2$.

The frequency ω_2 given by (6) which enters in χ_0 decreases as a function of the magnetic field, and reaches a minimum ω_{me} at the phase-transition point $H = H_{thr}$ ($\Phi = \pi/2$). The susceptibility χ_0 is then a maximum. In addition, the numerator of (13) is zero at $\Phi = 0, \pi/2$, and has a maximum at $\Phi \approx \Phi_1$. Correspondingly, the coefficient K is zero at $\Phi = 0$ or $\pi/2$ and a maximum at $\Phi = \Phi_1$ (see also Ref. 11 on this subject). The frequency ω_2 depends little on Φ owing to the large magnetoelastic gap in Dy.¹¹ Thus, for this domain structure the efficiency with which longitudinal ultrasound is excited is low in weak fields and in fields $H = H_{thr}$, but reaches a maximum in an intermediate field. Note that expression (13) can be obtained by using the conventional approach to problems of electromagnetic excitation of ultrasound: the purely electrodynamic problem for a magnet is first solved, after which account is taken of the coupling with the elastic subsystem by introducing the magnetoelastic coupling parameter ζ .

4.2. Generation of sound by displacement of domain walls

The analysis above is valid for a magnet in which the domain walls do not move. Yet in the absence of a constant magnetic field and in weak fields, Dy has a complicated domain structure consisting of six possible domain types. In the $\mathbf{H} \parallel \mathbf{h} \parallel \mathbf{y}, \mathbf{k} \parallel \mathbf{n} \parallel \mathbf{x}$ geometry such a domain structure exists up to a certain field $H = H_1$. In fields $H_1 < H < H_{thr}$ the domain structure is the one considered above, consisting of two domain types. The magnetization of a sample is via displacement of the domain walls in fields $0 < H < H_1$ and via rotation of the magnetization in the domains towards the direction of the external field in fields $H_1 < H < H_{thr}$. Equation (13) obtained above is thus valid only for fields $H_1 < H < H_{thr}$.

In the $\mathbf{H} \parallel \mathbf{h} \parallel \mathbf{x}, \mathbf{k} \parallel \mathbf{n} \parallel \mathbf{y}$ geometry the domains in which

the magnetization is directed counter to the external field are decreased in the course of the crystal magnetization, while the domains with magnetization directed along the field increase. At $H = H_1$ the sample becomes single-domain with a magnetization directed along the magnetic field. Thus, in this geometry the sample magnetization is due only to the displacement of the domain walls.

To explain ultrasound generation in the field region $0 < H < H_1$ instead of the Landau-Lifshitz equations we use in Eqs. (5), the equation of motion of a 180-degree domain wall in the Becker form.¹² Then, for example in $\mathbf{H} \parallel \mathbf{h} \parallel \mathbf{y}$ geometry, the ultrasound generation is described by the equations

$$\begin{aligned} m\ddot{v} + \kappa v &= M_s h_y - G D u_x, \\ \rho \ddot{u}_x &= c_{11} D^2 u_x + (2G/d) D v, \\ (1 - 1/2 i \delta^2 D^2) h_y + (8\pi M_s / d) v &= 0, \end{aligned} \quad (14)$$

where G and D are the averaged values of the magnetostriction constant and of the domain dimensions, v is the average displacement of the domain walls, and m and κ are the average mass and average elasticity coefficient of the domain walls. The boundary conditions in the system (14) are again the vanishing of the stresses on the magnet boundary and the continuity of the vectors \mathbf{E} and \mathbf{H} . Note that Eqs. (14) describe the excitation of inhomogeneous (flexural) oscillations of the domain walls, which in turn generate elastic oscillations.

It can be shown that the solution of the system (14) is given by expressions (8)–(12), in which

$$\chi = \frac{\chi_0 \omega_0^2}{\omega_0^2 - \omega^2}, \quad \zeta = \frac{G^2}{c_{11} M_s^2} \chi. \quad (15)$$

Here $\chi_0 = 2M_0^2 / \kappa d$ is the static susceptibility of the domain-wall displacement, $\omega_0 = (\kappa/m)^{1/2}$ is the frequency of the natural oscillations of the domain walls. Similar results are obtained also for the $\mathbf{H} \parallel \mathbf{h} \parallel \mathbf{x}, \mathbf{k} \parallel \mathbf{n} \parallel \mathbf{y}$ geometry.

The conversion coefficient (12) depends on the external magnetic field through the quantities d, m , and κ , which characterize the domain structure and the domain walls of the sample. The frequency ω_0 of the natural oscillations of the domain walls thus depends on H . According to (15), the dynamic susceptibility of the magnet, and hence the EMAT efficiency (12), can therefore have a resonant dependence on H . (According to estimates,¹³ ω_0 is in the range of tens and hundreds of megahertz.)

Assuming, as usual, the parameter ζ to be small compared with the permeability μ , we obtain for the transformation coefficient the equation

$$K = \text{const} \frac{\chi^2}{(1 + 4\pi\chi)^2}, \quad (16)$$

where χ is the susceptibility from (15). The increase of the EMAT efficiency as a function of H in the interval $0 < H < H_1$ can be attributed either to an increase of the static susceptibility χ_0 or to resonance of the domain walls at the frequency ω_0 of the natural oscillations of the domain walls.

It follows thus from the calculations that on the field dependences of EMAT in a ferromagnet there should be observed, first in weak fields, a generation peak due the displacement of the domain wall, and second, a region of in-

tense generation when the spins are reoriented in the domains (in the $\mathbf{H}\parallel\mathbf{b}$ configuration).

Experiment shows that for $T < T_1$ the $K(H)$ plots have maxima for both $\mathbf{H}\parallel\mathbf{a}$ and $\mathbf{H}\parallel\mathbf{b}$ of the EMAT efficiencies in weak fields (see Figs. 1 and 2), which terminate simultaneously when the magnetic susceptibility decreases [as evidenced by the decrease of the slopes of the $M(H)$ plots, curve 3 of Fig. 2]. It is natural to attribute this maximum to displacements of the domain walls in accordance with Eq. (16).

For $\mathbf{H}\parallel\mathbf{a}$, after the unfavorably located domains vanish, the sample is magnetized to saturation. In fact, the EMAT efficiency in fields stronger than H_1 is extremely small (curve 1 of Fig. 1). For $\mathbf{H}\parallel\mathbf{b}$, on the contrary, there should be observed a second maximum (or an entire region) where the EMAT is effective, a maximum due to spin-reorientation processes in the oblique phase [in accordance with (13)]. This maximum should terminate in the field H_{th} defined by Eq. (4). These conclusions agree well with experiment (curves 1 and 2 in Fig. 2). In the physical sense, the field H_{th} thus corresponds to the experimentally determined field H_2 .

To conclude this section we note that calculation of the EMAT efficiency in the region of a transition from an antiferromagnetic helical phase into a ferromagnetic fan phase entails considerable difficulties and was not performed in the present study. We assume, however, that the peak of the transformation has in this transition the same character as the peak, described earlier,⁹ of the transformation in the region of the transition from the paramagnetic to the ferromagnetic state.

5. MAGNETIC PHASE DIAGRAMS

To construct the magnetic phase diagrams of Dy in a field \mathbf{H} oriented in the basal plane, we also calculated the helicoidal antiferromagnetic structure of this metal with allowance for easy-plane anisotropy.

A calculation of such a structure in an hexagonal crystal, without allowance for anisotropy in the easy plane, was carried out earlier by Enz.¹⁴ The magnetic moments of each crystal plane, connected by strong exchange interaction, were described by a single azimuthal angle φ_i . A ferromagnetic exchange interaction was assumed between neighboring planes, and an antiferromagnetic between every other plane. It follows from this model that the destruction of the helicoidal structure by a magnetic field proceeds in two stages: in a field H_1 the helicoid is destroyed and a fan ferromagnetic structure is produced; with further increase of the field the fan angle decreases, and in a field $H_2 = 2.06 H_1$ the magnetic moments of the atoms are oriented along \mathbf{H} . From the experimental data⁴⁻⁶ it follows, however, that for $\mathbf{H}\parallel\mathbf{a}$ the destruction of the helicoid is not always accompanied by formation of a fan structure—at temperatures below 125 K the fan phase is apparently not realized in this orientation. At the same time, at $T > 140$ K the calculation¹⁴ is in satisfactory agreement with experiment.

It can be proposed that the vanishing of the fan phase as T_1 is approached is connected with the influence of the easy-plane anisotropy, which increases rapidly when the temperature is lowered.¹⁵ Since the period of the helicoid in Dy is about ten lattice periods, an analytic calculation of such a structure with allowance for easy-plane anisotropy is quite complicated. Numerical methods were therefore used to

find the energetically most favorable spin configuration.

We used an expression for the free energy in dimensionless variables

$$f = \sum_j \{ -\cos(\varphi_i - \varphi_{i-1}) + j \cos(\varphi_i - \varphi_{i-2}) - h \cos \varphi_i + k_6 \cos[6(\varphi_i - \psi)] \}, \quad (17)$$

where $k_6 \equiv K_6/I_1 M_s^2$ is the easy-plane anisotropy constant, I_1 is Enz's first exchange integral, $h \equiv H/I_1 M_s$, and ψ is the angle between the direction of \mathbf{h} and the \mathbf{b} axis of the basal plane. The value $j \equiv I_2/I_1 = 1/4 \cos(2\pi/11)$ was specified so that in the absence of anisotropy and a magnetic field a helicoid equal to 11 lattice periods arose. This corresponds to Dy at $T = 105$ K, when the constant of the easy-plane anisotropy K_6 is already quite large ($\sim 10^5$ erg·cm⁻³, Ref. 15).

The gradient-descent method was used with a computer to find the values of φ_i corresponding to the free-energy minimum f_{min} at given values of the parameters ψ , k_6 , and h . It turned out that, as a rule, all three main configurations of the magnetic moments—helicoid, fan, and oblique phases—correspond to local minima of f . For these configurations we calculated f_{min} as a function of k_6 and h for a specified ψ . The values of h and d_6 corresponding to the phase-separation boundaries were found as the intersection lines of the $f_{min}(k_6, h)$ traces for these phases. We have thus calculated the H - K_6 phase diagrams at the values thus calculated the H - K_6 phase diagrams at the values $\psi = 0, 2/3, 30^\circ$ (the last—for $\mathbf{H}\parallel\mathbf{a}$, the transition from $\psi = 0^\circ$ to 30° is equivalent to reversal of the sign of k_6).

Figure 4 shows similar diagrams for $\psi(2/3)^\circ$ (i.e., small deviation from the difficult axis \mathbf{b}) for $K_6 > 0$, and for $\psi = 30^\circ$ at $K_6 < 0$. It can be seen that with increase of the anisotropy the helicoidal structure is suppressed and at values $K_6/H_1^0 M_s \approx 1$ it is not realized at all (H_1^0 is the value of H_1 at $k_6 = 0$, i.e., the value used in the initial model¹⁴). A collinear ferromagnetic structure occurs at

$$H_2 = 2.06 H_1^0 + 36 K_6 / M_s. \quad (18)$$

It has turned out that the boundary between the fanfold and angle phase is extremely sensitive to disorientation of the magnetic field relative to the difficult axis ψ . The dashed line in Fig. 4 shows this boundary at $\psi = 0^\circ$; all the remaining phase boundaries at $\psi = 0$ and $(2/3)^\circ$ are practically the same.

It is seen from Fig. 4 that for $\mathbf{H}\parallel\mathbf{b}$ the helicoidal-angular-fanfold triple phase is determined by the condition

$$K_6/H_1^0 M_s \approx 0.3. \quad (19)$$

Control calculations for the values of j corresponding to helicoid periods equal to 18 and 9 lattice periods have shown that the general structure of the H - K_6 phase diagrams is preserved, and the values of $K_6/H_1^0 M_s$, corresponding to the triple point (19) and to total suppression of the helicoidal structure, differ by less than 10%. Thus, one can expect the foregoing conclusions to be valid for arbitrary real values of the helicoid period.

The foregoing interpretation of the field dependences of the EMAT efficiency can be used to construct the magnetic phase diagrams of Dy in a magnetic field oriented along the easy and difficult axes to the basal plane. To establish the boundaries of existence of various magnetic states, the inter-

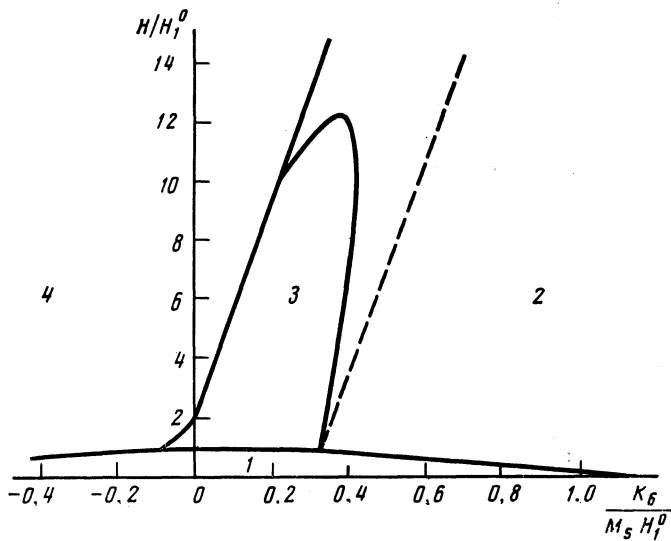


FIG. 4. Calculation of the phase diagram of Dy for $\psi = 30^\circ$ ($\mathbf{H} \parallel \mathbf{a}$) at $K_6 < 0$ and for $\psi = (2/3)^\circ$ at $K_6 > 0.1$ —helicoid, 2—angle phase; 3—fan phase; 4—collinear phase. Dashed—boundary between fan-fold and canted phase at $\psi = 0^\circ$ ($\mathbf{H} \parallel \mathbf{b}$).

nal magnetic field H in the sample was calculated with allowance for the temperature dependence of the saturation magnetization $M_s(T)$ (Ref. 4). The demagnetization factors of the samples are $N_a = 3.5(\mathbf{H} \parallel \mathbf{a})$ and $N_b = 1.9(\mathbf{H} \parallel \mathbf{b})$. They were calculated for a magnetic field at the center of the sample faces, on which the excitation and reception of elastic waves took place.

The magnetic phase diagrams of dysprosium constructed in this manner for $\mathbf{H} \parallel \mathbf{a}$ and $\mathbf{H} \parallel \mathbf{b}$ are shown in Figs. 5 and 6, respectively. With the internal magnetic field and temperature as coordinates, the boundary of the polydomain phase below T_1 practically coincides with the abscissa axis ($H_1 \ll 1$ kOe). The lower curve in Fig. 5 for $T_1 < T < T_2$ is the limit of the existence of the antiferromagnetic phase, while the upper is the limit of the existence of the fan ferromagnetic phase. The upper curve in Fig. 6 shows the H_2 dependence calculated from Eq. (18). In the calculation we used data on the temperature dependences of the saturation magnetization⁴ and the constants of the easy-plane anisotropy.¹⁵ It can be seen that the theoretical curve is in fairly good agreement with the experimental data. This makes it possible, in turn, to determine the magnetic-anisotropy constants

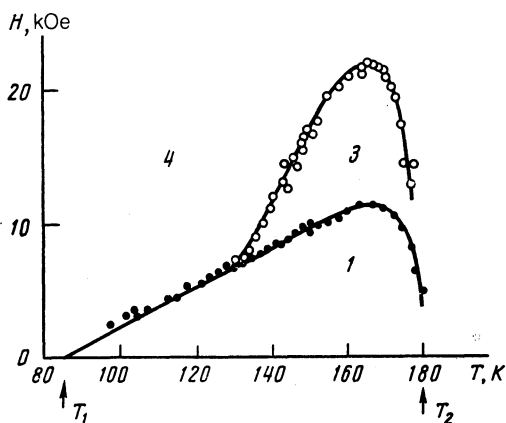


FIG. 5. Phase diagram of Dy for $\mathbf{H} \parallel \mathbf{a}$: 1—helicoid, 3—fan phase, 4—collinear phase, H —internal magnetic field. Experimental points: \bullet —field H_1 , \circ —field H_2 .

of metals from data on electromagnetic sound excitation.

In addition, the phase diagram for $\mathbf{H} \parallel \mathbf{b}$ (Fig. 6) also shows the boundary between the fan and oblique ferromagnetic phases. This boundary is constructed from the field dependences shown in Fig. 3, and corresponds to fields and temperatures at which the hysteresis processes on the $K(H)$ dependences are completed. To the left of this boundary the oblique phase occurs, and to the right apparently the fan phase. Note that according to (19) the triple point on the antiferromagnetic helicoid—ferromagnetic fan phase—ferromagnetic oblique phase triple point should be realized at $T \approx 90$ K. The experimentally observed interface is located near this temperature.

Thus, an experimental and theoretical investigation of EMAT in Dy has made it possible to indicate the main mechanisms responsible for ultrasound generation in this metal. In a polydomain ferromagnetic phase at $T < T_1$ the main contribution to the EMAT efficiency is made by magnetoelastic interactions connected with displacement of domain boundaries and with rotation of the magnetization vectors in

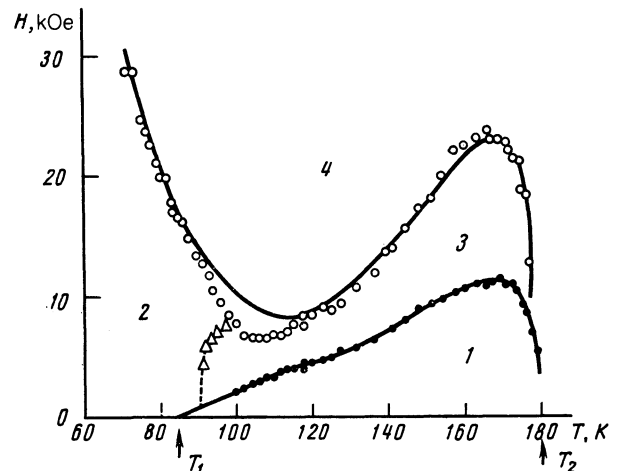


FIG. 6. The same for $\mathbf{H} \parallel \mathbf{b}$: 2—angle phase, upper line—calculated from Eq. (18), Δ —experimental points separating the region with $K(H)$ hysteresis from the region without hysteresis.

domains. In the interval $T_1 < T < T_2$ intense sound generation takes place on going from the spiral antiferromagnetic phase into the intermediate ferromagnetic phase, and also where an intermediate phase—angular or fan exists.

In conclusion, the authors are sincerely grateful to E. Fawcett for supplying the dysprosium single crystal, and also to M. I. Kaganov and R. Z. Levitin for constructive criticism.

¹A. N. Vasil'ev and Yu. P. Gaïdukov, *Usp. Fiz. Nauk* **141**, 437 (1983) [*Sov. Phys. Usp.* **26**, 952 (1983)].

²A. V. Andrianov, A. N. Vasil'ev, Yu. P. Gaïdukov, and R. S. Ilyasev, *Fiz. Met. Metall.* **67**, 708 (1989).

³K. P. Belov, M. A. Balyanchikova, R. Z. Levitin, and S. A. Nikitin, *Rare Earth Ferro- and Antiferromagnets* [in Russian], Nauka, 1965.

⁴R. Herz and H. Kronmuller, *J. Magn. Magn. Mat.* **9**, 273 (1978).

⁵M. Akhavan, H. A. Blackstead, and P. L. Donoho, *Phys. Rev. B* **8**, 4258

(1973) and S. B. Palmer, *J. Phys. F* **8**, 247 (1978).

⁷A. V. Andrianov, A. N. Vasil'ev, Y. P. Gaïdukov, and E. Fawcett, *Pis'ma Zh. Eksp. Teor. Fiz.* **49**, 621 (1989) [*JETP Lett.* **49**, 715 (1989)].

⁸M. B. Gitis, *Fiz. Tverd. Tela (Leningrad)* **14**, 3563 (1972) [*Sov. Phys. Solid State* **14**, 2992 (1972)].

⁹A. V. Andrianov, V. D. Buchel'nikov, A. N. Vasil'ev *et al.*, *Zh. Eksp. Teor. Fiz.* **94**, No. 11, 277 (1988) [*Sov. Phys. JETP* **67**, 2331 (1988)].

¹⁰Yu. I. Sirotnin and M. P. Shaskol'skaya, *Principles of Crystal Physics* [in Russian], Nauka, 1979.

¹¹E. A. Turov and V. G. Shavrov, *Usp. Fiz. Nauk* **140**, 429 (1983) [*Sov. Phys. Usp.* **26**, 593 (1983)].

¹²R. Becker, *J. Phys. Rad.* **12**, 332 (1951).

¹³A. G. Gurevich, *Magnetic Resonance in Ferrites and Antiferromagnets* [in Russian], Nauka (1974).

¹⁴U. Enz, *Physica* **26**, 698 (1960).

¹⁵D. J. Martin and J. J. Rhune, *J. Phys. C* **10**, 4123 (1977).

Translated by J. G. Adashko